Available online at www.sciencedirect.com
ScienceDirect
ELSEVIER
Journal of Crystal Growth 300 (2007) 538–550
JOURNAL OF CRYSTAL GROWTH
www.elsevier.com/locate/jcrysgro

Vertical optical floating zone furnace: Principles of irradiation profile formation

D. Souptel*, W. Löser, G. Behr

Leibniz-Institute of Solid State and Materials Research Dresden, PF 27 01 16, D-01171 Dresden, Germany

Received 19 September 2006; received in revised form 15 December 2006; accepted 18 December 2006
Communicated by P. Rudolph
Available online 16 January 2007

Abstract

The light distribution within the vertical double-ellipsoid mirror furnace applied for floating zone crystal growth with optical heating is studied. During the last few years, this setup was intensively applied for crystal growth of intermetallic and oxide materials due to its advantages for radiation focussing, which is superior in some key features compared to other commercial horizontal and vertical optical floating zone facilities. A point source model was used as a light source to reveal basic principles of the irradiation profile formation, which can strongly affect the melt flows, as well as the curvature and stability of crystallization front. Effects of the lamp displacement along the vertical optical axis with respect to the focal point of the lower elliptical mirror and the effect of mirror apertures were studied as the prime factors, which determine the light profile on the crystal. The efficiency of the light focusing in the presented optical configuration is discussed.
© 2007 Elsevier B.V. All rights reserved.

PACS: 01.50.My; 81.10.Fq

Keywords: A1. Computer simulation; A1. Radiation; A2. Floating zone technique; A2. Mirror furnaces

1. Introduction

The floating zone (FZ) technique with optical heating is a widely used method for crystal growth for research purposes. This container-free technique has become a preferred growth method for various classes of oxides and intermetallics, especially for those showing extreme melt reactivity and high melting temperatures. Commercial facilities use, as a rule, ellipsoid mirrors for focusing of the light emitted from halogen or xenon lamps. A radiation source is located in one focal point of the ellipsoid of revolution, and the molten zone in the other focal point. The crystal growth process proceeds always in vertical direction. The basic optical configurations of FZ facilities can be subdivided into two classes: horizontal and vertical optical arrangements, respectively.

In horizontal optical configurations, the major ellipsoid axes (axes of revolution) are in a horizontal plane, where both foci of the ellipsoid are located. The crystal is moved and the crystallization process of the molten zone proceeds along the perpendicular (vertical) axis [1–4]. In this class fall commercial FZ optical systems consisting of one- or two-ellipsoid mirrors (NEC Machinery Co., Japan) or four-ellipsoid mirrors (Crystal Systems, Inc., Japan) [5,6]. The mirrors are arranged in a plane around the growing crystal. The lamps are positioned in the 1st focal points of the respective mirrors whereas all the 2nd focal points coincide with the molten zone position. Such optical systems are used in many research institutes worldwide and show good optical efficiency of radiation focussing [3,7–9].

In vertical optical configurations, the axes of revolution of the elliptical mirror(s), of the growing crystal, and of molten zone coincide. In this case, a single lamp is positioned in one focal point of the elliptical mirror. There are two principal available types of these optical FZ

*Corresponding author. IFW Dresden, Postfach 270016, D-01171 Dresden, Germany. Tel.: +49 351 4659 756; fax: +49 351 4659 480.
E-mail address: d.suptel@ifw-dresden.de (D. Souptel).

0022-0248/$ - see front matter © 2007 Elsevier B.V. All rights reserved.
doi:10.1016/j.jcrysgro.2006.12.042

facilities, the closed mono-ellipsoid [10,11] and the vertical double-ellipsoid mirror furnaces (MPEI, Russia) [12–14], respectively. The first one was widely used in microgravity experiments on manned and unmanned space flights. It consists of one hollow elliptical mirror where the lamp and the growing crystal are situated one over another in this cavity.

The vertical double-ellipsoid mirror furnace, in spite of more then 20 years commercial supply, up to now did not find a widespread application. Nevertheless, in the past 5 years there is a jump in the number of publications from various groups on single crystal growth of oxide and intermetallic compounds with this FZ facility [12–22]. Its optical scheme provides grave practical advantages for radiation focussing, which is superior in some key features compared to other horizontal and vertical optical FZ facilities. Since, to our knowledge, no studies of this optical scheme exist we would like to fill a gap and describe the intrinsic features of the radiation flux in this vertical double-ellipsoid mirror furnace.

In the present work, we show results of a simulation of ray propagation from the lamp to the crystal and radiation profiles at the crystal surface for a point source model to reveal the intrinsic "focusing" features of this optical system, which is more complex than FZ facilities with horizontal or mono-ellipsoid vertical optical configurations, which were already subjected to similar studies [4,23–25]. The basic accent is put on a variation of the lamp position with respect to the focal point of the first (lower) mirror. It will be shown that the irradiation profiles display unexpected singularities due to the complex behaviour of the rays after two reflections from the two elliptical mirrors, which must be taken into account for construction of auxiliary components within the apparatus and the optimization of FZ growth processes. The presented data will help to understand the basic principles of practical optical alignment and adjustment of the apparatus for predefined crystal growth requirements.

2. Practical advantages of the vertical double-ellipsoid optical scheme

The optical scheme of a vertical double-ellipsoid configuration of FZ setup is shown in Fig. 1a. In practice, a 3 or 5 kW air-cooled xenon arc lamp positioned at the focal point F1 of the lower mirror is used as the irradiation source (see Fig. 1b). The molten zone is located inside the crystal growth chamber at the focus F4 of the upper mirror. The FZ process proceeds by vertical pulling (downwards or upwards) of the feed rod and the growing crystal. The radiation power is controlled by both the lamp electrical power and a 4-sector mechanical flux shutter positioned between the mirrors (see Fig. 1a). Here, on the basis of a huge number of FZ growth experiments with various materials [12–19,22], the fundamental practical advantages of the presented optical scheme are summarized for the first time as a background of theoretical investigations of light propagation within the present FZ setup in order to optimize parameters for specific crystal growth purposes.

- Axial symmetry of this optical configuration provides extreme uniform azimuthal heating of the melting zone. It permits to control the irradiation power range absorbed by the crystal surface from 0 to 100% by both mechanical flux shutter and electrical power of the arc lamp.
- Due to the large size of the upper mirror (~600 mm) and the narrow bundle of rays illuminating the molten zone mainly from above, there is an easy access to the crystal growth chamber, even during the growth process, and sufficient space for mounting of auxiliary functional components in the neighbourhood of the growth chamber (e.g. afterheater for growing crystal, pyrometer, camera, [12]) without any appreciable radiation absorption.
- Another feature of the vertical optical configuration is the narrow region of possible incident radiation angles Θ_3 onto the crystal $<70^\circ$ (see Fig. 1b) due to the cut-off by the mirror (instead of almost 140–180° for horizontal optical configurations) [3,4]. This enables much shorter quartz tubes for the growth chamber (typically: 60 mm in length [22] instead of ~350 mm [5,6]) The shorter quartz tube permits the application of higher gas pressure, for example, 100 bar for quartz tubes with 14 mm wall thickness and 60 mm length [22,26].
- The very high efficiency of the radiation flux focusing was confirmed for crystallization of refractory materials. In practice only one 5 kW (electrical power) xenon lamp is required for melting refractory oxides with ~2800 °C melting temperature [13]. By contrast, four 3 kW xenon lamps (12 kW in total) are necessary for achieving similar temperatures in four-mirror horizontal optical furnaces [9]. We connect this practical result with more effective focussing of the light flux emitted by the arc lamp and a narrower light profile on the crystal surface. For example, the width of the illuminated area can be as small as ~1 mm for the presented optical scheme, as will be shown further, in comparison to 5 mm for the horizontal optical scheme [23] for a point source model.

The basic disadvantage of the presented optical configuration is the more sophisticated alignment procedure of the lamp and the mirrors than for commercial FZ setups with horizontal optical arrangement. The full exploitation of practical features of the current vertical double-ellipsoid configuration requires further detailed theoretical studies and is not presented in this issue.

3. Geometry parameters of the optical configuration

The optical scheme (see Fig. 1b) consists of two mirror segments of ellipsoids of revolution with the semiaxes a_1, c_1 and a_2, c_2, focal sizes p_1 and p_2 and eccentricities e_1 and e_2

of the lower and the upper mirror, respectively. The c-axes are directed along the z-axis of Cartesian coordinates coinciding with the optical axis, but a-semiaxes are parallel to the horizontal (x, y) plane. The mirror segments are obtained by cutting corresponding ellipsoids parallel to the (x, y) plane at fixed z, generating apertures with inner and outer diameter D_{in} and D_{out}, or in terms of zenith observation angle Θ_{in} and Θ_{out} with respect to the corresponding ellipsoid foci (see Fig. 1b), respectively. In the inner aperture ($D_{1,in}$) near the vertex of the lower mirror, the mechanical containment and the electrical junction of the lamp are mounted, whereas the inner aperture ($D_{2,in}$) of the upper mirror contains the crystal growth chamber (see Fig. 1a). $D_{1,out}$ and $D_{2,out}$ define the outer sizes of the mirrors. The apertures play a role as cut-offs for the radiation flux. All mirror parameters are presented in Table 1.

For simplicity, in the presented optical scheme the 2nd focal points (F2 and F3) of the upper and lower ellipsoids as well as the origin of the coordinates are considered to coincide (see Fig. 1). Accordingly, the positions of the foci and the vertices of the lower and upper mirror are $-2p_1 = -2\sqrt{c_1^2 - a_1^2}$, $S_1 = -c_1 - p_1$ and $2p_2 = 2\sqrt{c_2^2 - a_2^2}$, $S_2 = c_2 + p_2$, i.e. -792, -866 and $+1008$, $+1159$ mm, respectively. This leads to a total distance of 2025 mm between vertices of the mirror ellipsoids, which basically determines the height of the FZ growth facility.

A cylinder of diameter $D_{crystal} = 10$ and 100 mm length was applied as the crystal model. Its centre is positioned at

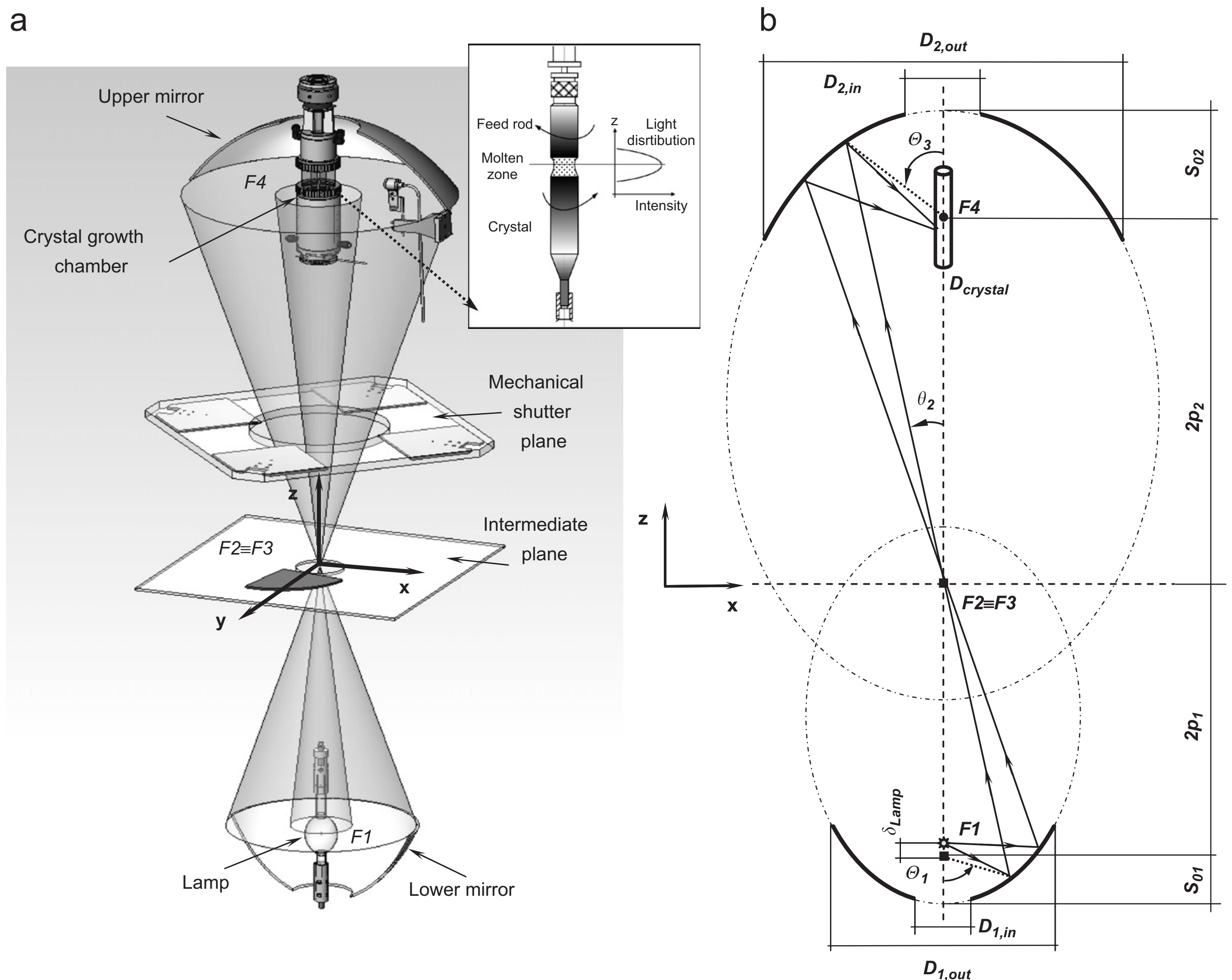

Fig. 1. Scheme (a) and optical configuration (b) of the vertical optical FZ furnace. The inset to (a) is a sketch of the FZ crystal growth process with corresponding light profile at the crystal surface. F1, F2 and F3, F4 are focal points of lower and upper ellipsoids and $2p_1$ and $2p_2$ are distances between them, respectively (in the present case F2 and F3 coincide). The lamp position is shifted from the focus F1 at the distance δ_{Lamp}. The quantities $D_{1,in}$, $D_{1,out}$ and $D_{2,in}$, $D_{2,out}$ are the inner and outer apertures of the lower and upper mirror, respectively, and Θ_1 and Θ_3 are zenith observation angles of the corresponding mirror surface elements from points F1 and F4, respectively. θ_2 is the angle between the optical axis and the light ray after reflection from the lower mirror. The distances S_{01} and S_{02} are explained in text.

Table 1
Parameters of the elliptical mirrors used in calculations

Parameter	Lower mirror (1)	Upper mirror (2)
$a_{1,2}$ (mm)	253	418
$c_{1,2}$ (mm)	470	655
$p_{1,2} = \sqrt{c_{1,2}^2 - a_{1,2}^2}$ (mm)	396	504
$e_{1,2} = p_{1,2}/a_{1,2}$	0.84	0.77
$S_{01,02} = c_{1,2} - p_{1,2}$ (mm)	74	151
$S_{1,2} = c_{1,2} + p_{1,2}$ (mm)	866	1159
Mirror height (mm)	119	185
$\theta_{1,2\,\mathrm{in}}/D_{1,2\,\mathrm{in}}$	49°/132 mm	25°/137 mm
$\theta_{1,2\,\mathrm{out}}/D_{1,2\,\mathrm{out}}$	109°/348 mm	98°/587 mm

$a_{1,2}$, $b_{1,2}$, $p_{1,2}$ and $e_{1,2}$ are semiaxes lengths, focal size and eccentricity of the corresponding ellipsoids. S_{01}, S_{02} are the distances from ellipsoid vertex to focal points F1 and F2, respectively. S_1, S_2 are coordinates of the corresponding ellipsoid vertexes. Θ_{in}, D_{in} and Θ_{out}, D_{out} are the apertures defined by angle or diameter.

the focal point F4 and its axis coincides with the optical axis (z-axis). A point source situated near the focal point F1 of the lower mirror is used as a model of a lamp. Its position can be shifted from the focal point F1 by the distance δ_{Lamp}. It is varied in the present calculations in the range ± 18 mm. A positive displacement $\delta_{\mathrm{Lamp}} > 0$ means a lamp position above F1. The distance of the lamp from the vertex of the lower mirror is $S_{01} = c_1 - \sqrt{c_1^2 - a_1^2} + \delta_{\mathrm{Lamp}}$ and for $\delta_{\mathrm{Lamp}} = 0$ $S_{01} = 74$ mm. XBO 5 kW (electrical power) xenon arc lamp emits 750 W of radiation and this value was used in the presented calculations. The light emitted by the source is reflected by the lower mirror and converges at the intermediate plane near the focal points F2≡F3 (see Fig. 1). Then, the diverging bundle is again reflected by the upper mirror and finally converges near its focal point F4.

Further, we define the quantities Θ_1 and Θ_3 as the zenith observation angles of the mirror elements with respect to the foci F1 and F4, and θ_2 corresponding to the direction of the light ray propagation with respect to the optical axis (see Fig. 1b). The positive variations of the corresponding angles are shown in Fig. 1b.

4. Principles of calculation

In the computing-intensive Monte Carlo simulation, a large number of photons (up to 10^6) is necessary for ray tracing to obtain a smooth and statistically meaningful result, which qualifies the method with a more complex heat transfer for crystal growth as impractical. Alternatively, we utilized principles of geometrical optics to calculate the propagation of light emitted by the point source within every small solid angle element until it reaches the crystal surface after reflection from the two mirrors. The limitations of the geometrical optics at light focusing will be smoothed by a special integration of the irradiation profiles based on the principles that is more suitable for most practical applications.

The following approximations and simplifications are applied for modelling of the radiation flux distribution in the optical system: (i) the model is based on the approximations of geometrical optics; (ii) the lamp is considered as a point irradiation source emitting isotropically, i.e. a Lambert point source; (iii) diaphragms in practice situated at the intermediate and shutter planes, the aperture of the crystal growth chamber and of the lamp mechanical parts (see Fig. 1a), the effects of a quartz housing of the lamp and of the quartz tube of the crystal growth chamber are supposed to cause no principal changes in the irradiation profile formation and are not considered in the present issue; (iv) the reflectance of the mirrors is supposed to be unity, i.e. the absorption by the mirrors is neglected; and (v) higher order reflections are ignored, i.e. any ray is reflected from the mirrors only one time. According to our estimations, higher order reflections can change the irradiation profiles by less then 5%. All details of the present calculations are given in Appendix A.

5. Results and discussions

For understanding the principal features of the considered optical system, the basic phenomena at different stages of the light transmission from the point source toward the lower mirror, then to the upper mirror and finally to the crystal are considered in relation to the lamp position δ_{Lamp} with respect to the focal point F1.

5.1. Analytical calculation of the light profile on the crystal surface

In the degenerated case, if the lamp is situated directly in the focus (F1) of the lower mirror ($\delta_{\mathrm{Lamp}} = 0$) and the foci of the lower (F2) and the upper (F3) mirror coincide, the radiation profile on the crystal surface can be obtained in an analytical form in the same way as for the one-elliptical mirror furnace [24]. All the governing equations are presented in Appendix B.

The bell-shaped intensity distribution on the crystal surface for mirror shapes, which are not restricted by the segment apertures is presented in Fig. 2 (solid line). As expected, the narrow curve exhibits a single maximum at $z = 1010$ mm very close to the coordinate of the focus F4 $2p_2 = 2\sqrt{c_2^2 - a_2^2} = 1008$ mm (see Table 1). A simulated curve (dots) for the case of $\delta_{\mathrm{Lamp}} = 0$ and restricted size of the lower mirror by $D_{1,\mathrm{out}}$ is shown too. (The calculation is described in the subsequent sections.) Good coincidence of the analytical and simulated curves validates the simulated results. However, only a part of the analytical result can be reproduced by the simulated curve, because of the radiation cut-off by the lower mirror aperture $D_{1,\mathrm{out}}$.

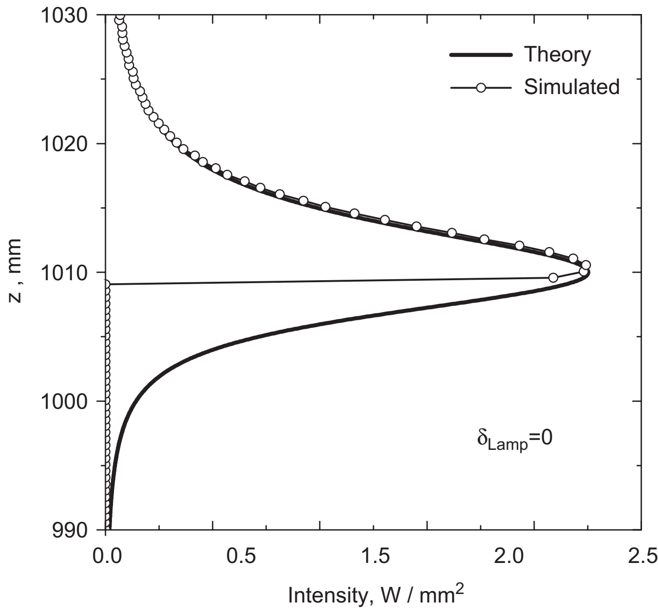

Fig. 2. Theoretical (solid line) and simulated (dots) light intensity distribution on the crystal surface for the case of lamp position in the focus F1 ($\delta_{\mathrm{Lamp}} = 0$).

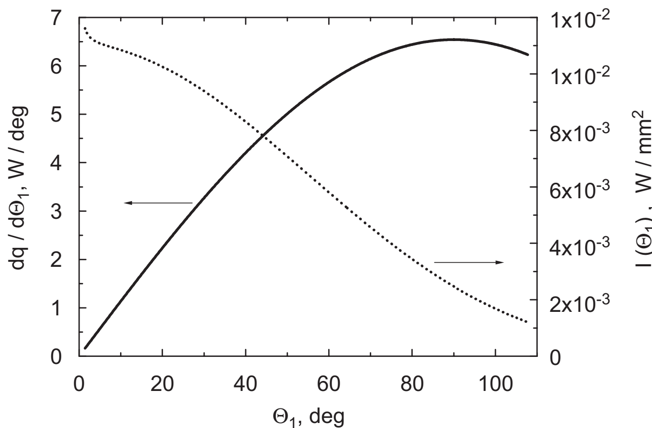

Fig. 3. Flux density $\mathrm{d}q/\mathrm{d}\Theta_1$ and light intensity $I(\Theta_1)$ across the lower mirror surface.

5.2. Radiation efficiency of the mirrors

Since the mirrors are only segments of the corresponding ellipsoids, it is very important to guarantee a high efficiency of the radiation transmission within the experimental setup and to minimize radiation losses caused by mirror surface geometry, especially of the lower mirror. In Fig. 3, the radiation flux density distribution $\mathrm{d}q/\mathrm{d}\Theta_1$ and radiation intensity $I(\Theta_1)$ across the lower mirror are shown. The flux density in our case is the light power reflected from the ring mirror segment between Θ and $\Theta + \mathrm{d}\Theta$. It is a more important parameter for estimating the energy efficiency of the mirror than the light intensity $I(\Theta)$ at the mirror surface itself, because it shows the energy contribution of every mirror element with respect to the reflected light. For an arbitrary $I(\Theta)$ on the mirror surface, the flux density can be written as:

$$\frac{\mathrm{d}q}{\mathrm{d}\Theta} = I(\Theta) f_0(\Theta), \tag{1}$$

where $f_0(\Theta) = 2\pi c^2((1-e^2)^2/(1+e\cos\Theta)^3)\sqrt{1+e^2+2e\cos\Theta}\sin\Theta$.

Here, $f_0(\Theta)$ is a normalization factor for an ellipsoid of revolution with larger semiaxis c and eccentricity e if the vertices of zenith angles Θ are at a focal point of the ellipsoid. In the degenerated case when a specific light profile $I(\Theta_1)$ at the lower mirror surface resulted from a point source of the total radiation lamp power P_0 positioned at the same ellipsoid focal point F1 as the vertices of Θ_1 angles, the flux distribution can be reduced to

$$\frac{\mathrm{d}q(\Theta_1)}{\mathrm{d}\Theta_1} = \frac{P_0}{2}\sin\Theta_1.$$

Variation of the lamp position within the range $\delta_{\mathrm{Lamp}} = \pm 10\,\mathrm{mm}$ does not strongly affect the result shown in Fig. 3.

It is easy to see that the energy efficiency of the inner regions of the lower mirror ellipsoid (near its vertex) is rather low and the aperture $D_{1,\mathrm{in}}$ corresponding to small angles Θ_1 does not strongly affect the total radiation power reflected (see Fig. 3). The outer region of the mirror, in spite of the irradiation intensity almost one order of magnitude lower, has a larger radiation flux density, i.e. more power is reflected from outer ring mirror segments. Hence, the largest contribution to the irradiation on the crystal comes from the outer part of the lower mirror surface.

Integration of Eq. (1) over the lower and upper mirror surfaces results in the conclusion that they reflect ~49% and ~52% of the total light flux, if a lamp would positioned at their focal points F1 and F4, respectively. These results are surprising according to the fact that the lower and upper mirror segments cover only 10% and 12.4% of the total surface area of the corresponding ellipsoids of revolution, respectively. Nevertheless, mirror efficiency is defined not by the mirror area but mainly by the field-of-vision angle of the mirror surface with respect to the point of the lamp position. In our case, these are 49–109° and 25–98° for lower and upper mirrors (see Table 1), respectively, and covering the most effective angle ranges of the light energy reflection. Moreover, the present optical parameters and apertures of the mirrors were adjusted in such a way that for the appropriate lamp positions near the focal point F1 there are almost no additional energy losses at the upper mirror and the whole light power reflected by the lower mirror is incident at the crystal (melt) surface as will be shown below.

5.3. Light propagation from the lower to the upper mirror

Modelling of the light ray propagation between the mirrors is a basis of practical alignment, adjustment and

efficiency of the optical system, which can also be affected by construction parts mounted between the mirrors (see Fig. 1a). Here, only the exterior aperture $D_{1,out}$ of the lower mirror will be considered, unless otherwise specified, to reveal the ray traces in the optical system.

The ray distribution θ_2 vs. Θ_1 of the light reflected from the lower mirror is presented in Fig. 4 for various lamp positions δ_{Lamp}. The higher the lamp position δ_{Lamp} is the larger is the range of θ_2 angles, i.e. the wider is the bundle

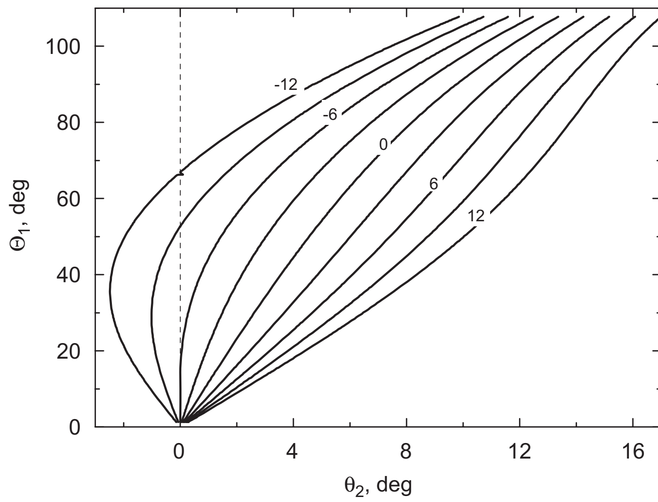

Fig. 4. Ray distribution θ_2 vs. Θ_1 of the light reflected from the lower mirror for various lamp positions $\delta_{Lamp} = -12, -9, \ldots, 9$ and 12 mm. Θ_1 axis is in the vertical direction corresponding to appropriate positions of the lower ellipsoid elements.

of light rays reflected from the lower mirror. Also, for high negative values of δ_{Lamp} there are light rays near the lower mirror vertex (small Θ_1) with negative θ_2. That means that these rays do not cross the optical axis as shown in Fig. 1b but form a divergent beam of rays. The effect is visible in the shape of the cylinder symmetrically enveloping surface of the light rays propagated from the lower to the upper mirror illustrated by a cross-section in the vertical (x, z) plane in Fig. 5. The sections of the upper and lower mirror are also visualized. For $\delta_{Lamp} < 0$ (Fig. 5a), the bundle of rays is less divergent than for $\delta_{Lamp} \geqslant 0$ (Fig. 5b). For $\delta_{Lamp} < 0$, the light propagates close (and nearly parallel) to the optical axis and covers only the region near the vertex of the upper mirror. Vice verss, the higher the lamp position is the wider and more divergent becomes the light beam, which covers preferably the outer range of the upper mirror surface for $\delta_{Lamp} > 0$ (Fig. 5b).

The narrowest size of the enveloping surface between the mirrors is a so-called beam waist. Its size R_{waist} and position Z_{waist} as functions of δ_{Lamp} are presented in the inset of Fig. 5b. As expected, if the lamp is situated at F1 ($\delta_{Lamp} = 0$), $R_{waist} = 0$ and $Z_{waist} = 0$ is valid (i.e. the waist is at the focal point F2). The beam radius increases rapidly for negative $\delta_{Lamp} < 0$ but only moderately for $\delta_{Lamp} > 0$. Moreover, the waist position with respect to the focal point F2 rises from -350 to $+450$ mm for a shift in δ_{Lamp} from $+18$ to -8 mm. A bigger jump in the position of the beam waist is caused by the more complex pattern of the beam envelope surface for $\delta_{Lamp} < 0$ than for $\delta_{Lamp} > 0$ as obviously seen for $\delta_{Lamp} = -6$ mm in Fig. 5a.

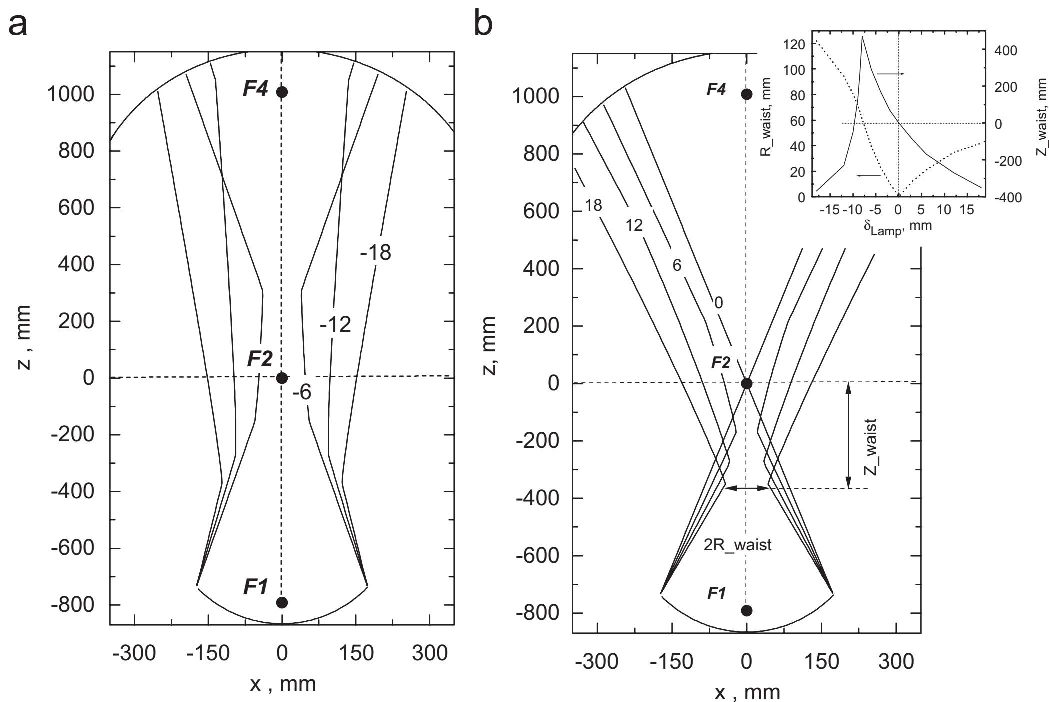

Fig. 5. Longitudinal section in the (x, z) plane of the light envelope surface between the mirrors for various lamp positions $\delta_{Lamp} < 0$ (a) and $\delta_{Lamp} > 0$ (b). Positions of foci F1, F2≡F3 and F4, the sections of the both mirrors as well as the radius and position of the beam waist (R_{waist} and Z_{waist}) are shown. Inset to (b): dependence of the radius of the enveloping surface waist R_{waist} (dotted line) and its position Z_{waist} (solid line) on the lamp position δ_{Lamp}.

Similar shapes of the beam envelope surfaces of the light propagated between the mirrors can be visualized often in practice and applied for light adjustment in the FZ setup because it is a basic precise indirect measure of the lamp position with respect to the focus F1.

5.4. The light reflection from the upper mirror

The light reflection from the upper mirror strongly changes the sequence of rays in the optical system. From this viewpoint, the optical system with two ray reflections is much more complex in comparison with optical schemes with a single reflection described in Refs. [4,23]. In Fig. 6a, the ray distribution on the upper mirror surface Θ_3 vs. Θ_1 is shown for various lamp positions δ_{Lamp}. With lowering of δ_{Lamp}, the range of Θ_3 decreases, i.e. less area of the upper mirror is illuminated (comparable with Fig. 5). A more important fact: beyond a critical value $\delta_{\mathrm{Lamp}}^{\mathrm{crit}}$ (<0) the rays leaving the upper mirror surface can be subdivided into two classes called "ordinary" and "overlapping" rays displaying positive and negative angles Θ_3, respectively (see Fig. 6a). For $\delta_{\mathrm{Lamp}} > \delta_{\mathrm{Lamp}}^{\mathrm{crit}}$, from each point of the upper mirror only one ray is reflected specified by Θ_3. For $\delta_{\mathrm{Lamp}} < \delta_{\mathrm{Lamp}}^{\mathrm{crit}}$, for the same point of the upper mirror in a region close to its vertex two rays from different elements of the lower mirror corresponding to different Θ_1 are incident and reflected. The two different pathways of such rays are illustrated in Fig. 6b and c. Rays with positive Θ_3 (classified as "ordinary" rays) incident from the opposite side of the lower mirror ($\Theta_1 > 0$) are superposed with rays with negative Θ_3 (classified as "overlapping" rays) incident from the same side of the lower mirror ($\Theta_1 < 0$). The critical value $\delta_{\mathrm{Lamp}}^{\mathrm{crit}}$ of lamp position for which overlapping appears depends on mirror ellipsoid parameters and in our case $\delta_{\mathrm{Lamp}}^{\mathrm{crit}} = -4.2$ mm.

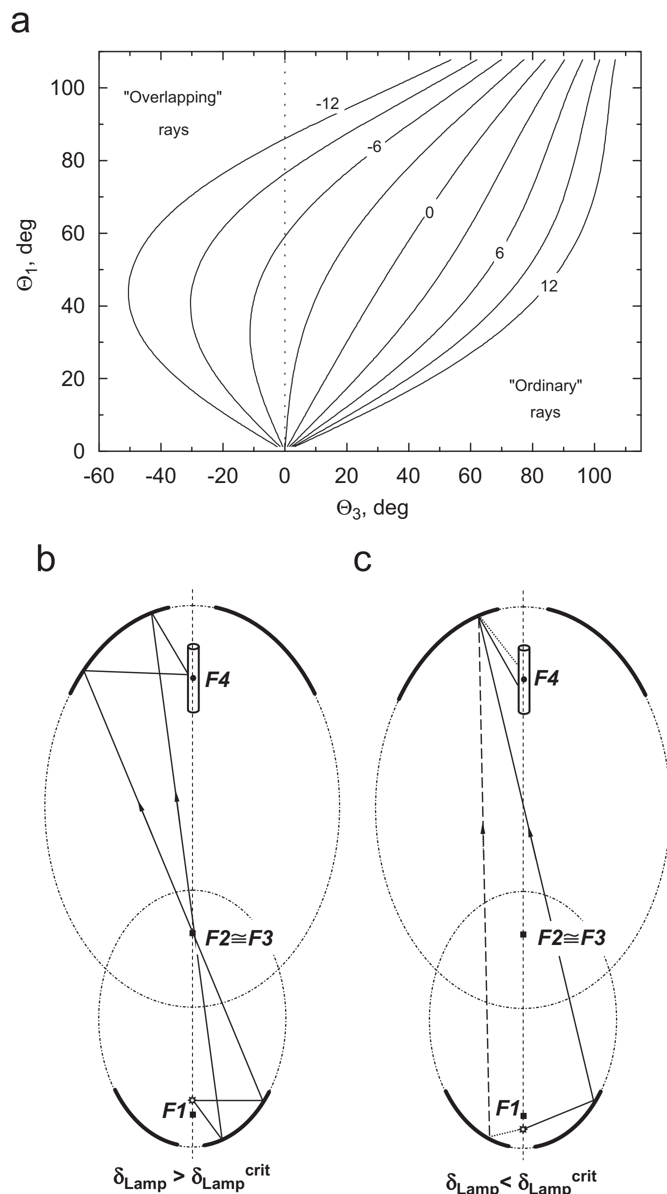

Fig. 6. Ray distribution Θ_3 on the upper mirror surface vs. Θ_1 for various lamp positions $\delta_{\mathrm{Lamp}} = -12, -9, \ldots, 9$ and 12 mm (a). The dotted line divides the Θ_3 angle range corresponding to "ordinary" and "overlapping" rays. Selected ray paths for small and large Θ_1 angles for the lamp positions $\delta_{\mathrm{Lamp}} > \delta_{\mathrm{Lamp}}^{\mathrm{crit}}$ (b) and $\delta_{\mathrm{Lamp}} < \delta_{\mathrm{Lamp}}^{\mathrm{crit}}$ with "ordinary" ray (solid line) and "overlapping" ray (dotted line) (c).

Light flux densities $\mathrm{d}q/\mathrm{d}\theta_3$ on the upper mirror surface as a function of Θ_3 are shown in Fig. 7 and play an important role in practice for indirect visual control of the real lamp position. If all rays are "ordinary", i.e. for $\delta_{\mathrm{Lamp}} > \delta_{\mathrm{Lamp}}^{\mathrm{crit}}$ (Fig. 7a) with increasing δ_{Lamp} the maximum position $\Theta_3^{\max}$ of the light flux profile moves to the margin of the upper mirror. For example, for $\delta_{\mathrm{Lamp}} = 12$ mm 75% of the total flux is constrained to the small interval $90^\circ < \Theta_3 < 107^\circ$. In the case with superposition of "ordinary" and "overlapping" of the rays, i.e. $\delta_{\mathrm{Lamp}} < \delta_{\mathrm{Lamp}}^{\mathrm{crit}}$ (Fig. 7b), almost the entire total flux is constrained in a region close to the vertex of the upper mirror. Its maximum position $\Theta_3^{\max}$ at the upper mirror surface corresponds to singular point of partial exact light focussing onto the upper mirror surface. The dependence of $\Theta_3^{\max}$, the position of the flux density maximum on the upper mirror, on the lamp position δ_{Lamp} is shown in the inset of Fig. 7a. As it was expected for $\delta_{\mathrm{Lamp}} = \delta_{\mathrm{Lamp}}^{\mathrm{crit}}$, the condition $\Theta_3^{\max} = 0$ is valid.

5.5. Light irradiation profiles at the crystal surface

The resulting irradiation distribution on the crystal surface is the decisive quantity for the crystal growth process. The ray distributions on the crystal surface 10 mm in diameter as functions of Θ_1 and Θ_3 are shown in Fig. 8a–d for both cases $\delta_{\mathrm{Lamp}} > \delta_{\mathrm{Lamp}}^{\mathrm{crit}}$ and $\delta_{\mathrm{Lamp}} < \delta_{\mathrm{Lamp}}^{\mathrm{crit}}$, respectively. It is worth reminding that only the exterior aperture of the lower mirror $D_{1,\mathrm{out}}$ was considered. In the case of $\delta_{\mathrm{Lamp}} > \delta_{\mathrm{Lamp}}^{\mathrm{crit}}$ the distribution function is always continuous (see Fig. 8a,b) although at one selected z-coordinate of the crystal surface for $\delta_{\mathrm{Lamp}} > 6$ mm up to three rays can arrive from different parts of the upper or the lower mirror (e.g. for $\delta_{\mathrm{Lamp}} = 12$ mm). The turning

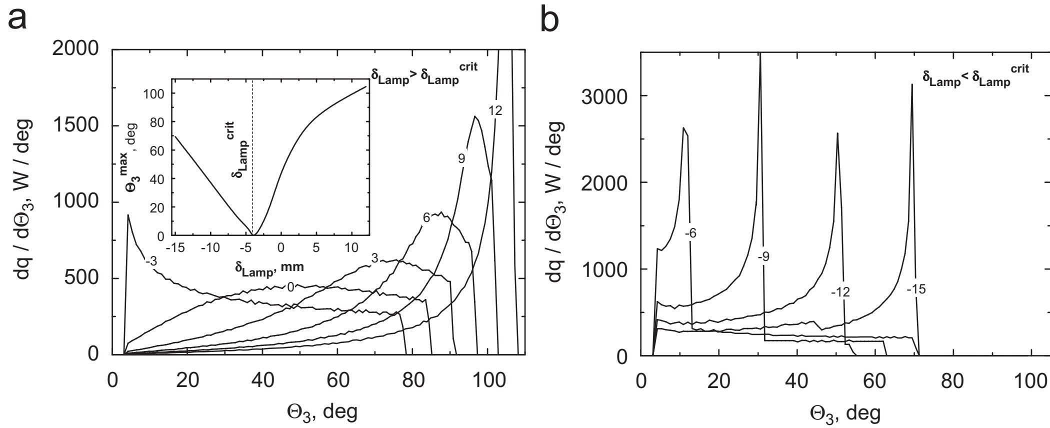

Fig. 7. Flux density $dq/d\Theta_3$ along on the upper ellipsoid surface for various lamp positions for the cases $\delta_{\text{Lamp}} > \delta_{\text{Lamp}}^{\text{crit}}$ (a) and $\delta_{\text{Lamp}} < \delta_{\text{Lamp}}^{\text{crit}}$ (b). Inset: zenith angle $\Theta_3^{\max}$ of the flux density maximum position on the upper mirror vs. lamp position δ_{Lamp}.

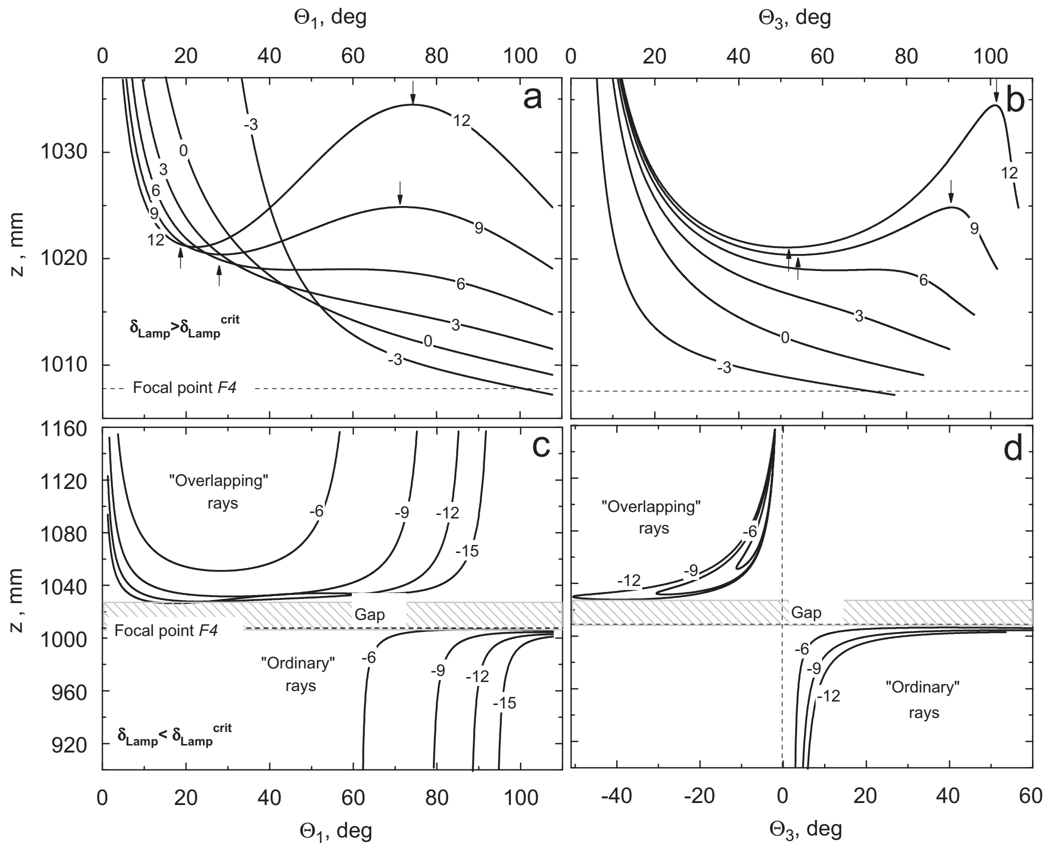

Fig. 8. Ray distributions on the crystal surface as functions of Θ_1 and Θ_3 for various lamp positions for the cases of $\delta_{\text{Lamp}} > \delta_{\text{Lamp}}^{\text{crit}}$ (a, b) and $\delta_{\text{Lamp}} < \delta_{\text{Lamp}}^{\text{crit}}$ (c, d). Arrows denote the "turning" points of the ray sequence. The inherent gap between the regions of "overlapping" and "ordinary" rays is hatched. The position of focal point F4 is marked as a dashed line.

points, where the direction of the ray sequence changes to the opposite direction, are denoted by arrows. It is remarkable that almost all the rays are reaching the crystal surface at z-coordinates slightly above the focal point F4.

Ray distributions at the crystal surface in the case of $\delta_{\text{Lamp}} < \delta_{\text{Lamp}}^{\text{crit}}$ exhibit another unusual feature, namely an obvious gap on the crystal surface between the regions of incident "ordinary" and "overlapping" rays (Fig. 8c,d). Such kind of gap is inherent to the optical system consisting of two elliptical mirrors and is definitely not a result of the limited size of the mirror segments. The reason for "inherent gap" formation is the special pathway of the

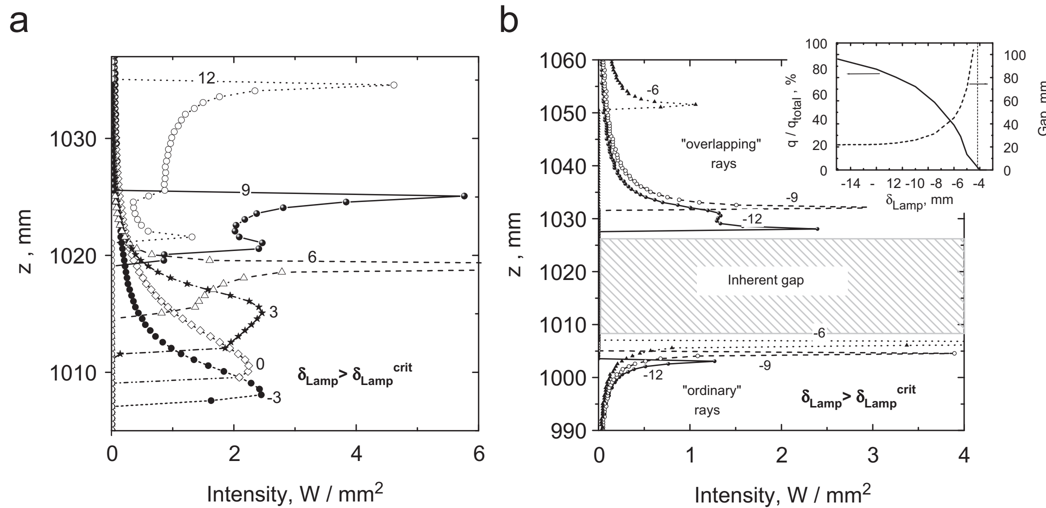

Fig. 9. Light intensity distribution on the crystal surface for various lamp positions δ_{Lamp} for the cases of $\delta_{\mathrm{Lamp}} > \delta_{\mathrm{Lamp}}^{\mathrm{crit}}$ (a) and for $\delta_{\mathrm{Lamp}} < \delta_{\mathrm{Lamp}}^{\mathrm{crit}}$ (b). The inherent gap between the "overlapping" and "ordinary" peaks is hatched. Inset to (b): gap width (dashed line) and the flux q in the "overlapping" peak with respect to the total flux reflected by the lower mirror q_{total} (solid line) as a function of lamp position δ_{Lamp}.

"overlapping" rays described in the previous sections and the upper limit of the z-coordinate of "ordinary" rays (see Fig. 8c,d).

Distributions of the rays arriving at the crystal surface presented in Fig. 8show the significance of the $\delta_{\mathrm{Lamp}}^{\mathrm{crit}}$ value and are also a prime factor for practical evaluation of the possible shadow fall on the light profile at the crystal and melt surfaces, caused by additional components of the FZ setup like the growth chamber, afterheater and pyrometer.

Light intensity profiles on a crystal surface are presented in Fig. 9. As shown in Fig. 9a for $\delta_{\mathrm{Lamp}} > \delta_{\mathrm{Lamp}}^{\mathrm{crit}}$, the higher the lamp position with respect to F1 the higher is the light profile itself and its intensity maximum position. The sharp edge of the light profiles for $\delta_{\mathrm{Lamp}} = -3$, 0 and 3 mm is caused by the exterior aperture $D_{1,\mathrm{out}}$ of the lower mirror. But the sharp jumps in the light profiles for the cases of $\delta_{\mathrm{Lamp}} = 6$, 9 and 12 mm are caused by intrinsic features of the light ray sequence at the crystal surface. They correspond to the turning points of the light rays denoted by arrows in Fig. 8a,b. At these points, the ray sequence is reversed (corresponding to the uniform variation of Θ_1 or Θ_3). By this phenomenon, a sharply restricted illuminated spot is formed at the crystal surface with extremely high intensity that is especially pronounced for $\delta_{\mathrm{Lamp}} = 6$ and 9 mm (see Fig. 9a). Outside this spot, the light intensity is one or two orders of magnitude lower. Thus, the self-collecting of the major light power (up to 98%) within a narrow definite range (<5 mm for 10 mm crystal diameter) with extremely sharp edges and very high average intensity is possible.

For $\delta_{\mathrm{Lamp}} < \delta_{\mathrm{Lamp}}^{\mathrm{crit}}$, two separate peaks appear, which are caused by "ordinary" and "overlapping" rays, respectively (see Fig. 9b). The inherent gap width between the peaks and the total flux within the "overlapping" peak is shown in the inset of Fig. 9b. For decreasing δ_{Lamp}, the distance between the peaks decreases down to its minimum (~20 mm) but the total flux in the "overlapping" peak rapidly increases. For instance, for $\delta_{\mathrm{Lamp}} = -5$ mm only 10% of the total flux is constrained to the peak caused by "overlapping" rays, compared with more than 85% for $\delta_{\mathrm{Lamp}} = -15$ mm. The width of the inherent gap depends also on the crystal diameter, mirror parameters and distance between the mirrors, which are not considered here in details.

In spite of the apparent practical necessity to avoid the case $\delta_{\mathrm{Lamp}} < \delta_{\mathrm{Lamp}}^{\mathrm{crit}}$, where a separation of the light incident onto the crystal into two beams occurs, these light profiles can become very effective for controlling the convection flow, especially Marangoni convection, because the temperature profiles can be designed by the individual peak intensity. Of course, only one of the two peaks should be selected by an appropriate construction of the crystal growth chamber. In spite of the energy losses, this can be very practical for FZ crystal growth of low melting materials such as various cuprates like $Sr_{14-x}Ca_xCu_{24}O_{41}$.

5.6. Exterior apertures of the mirrors

The limited segments of the mirrors form a light cone converging to the crystal and show a specific envelope shape depending on δ_{Lamp} and the size of apertures of the mirrors. Examples of such light cones converging near the crystal and the optical axis ($x = 0$) are presented in Fig. 10 for various lamp positions. For negative values of δ_{Lamp}, there is a pronounced effect of "self-focussing" of the converging light into a ring with a definite diameter denoted by arrows in Fig. 10. The illuminated area of such "focusing point" is finite and has width of 0.1–3 mm depending on the lamp position δ_{Lamp} and will be called the

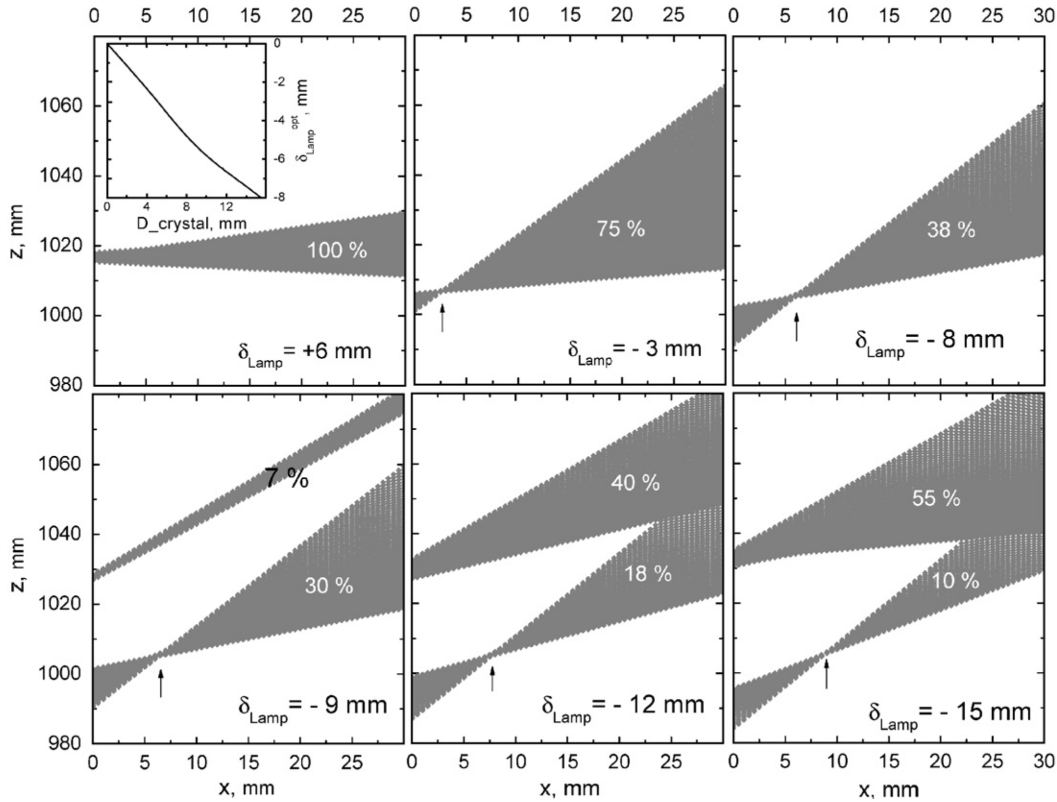

Fig. 10. Shape of converging light beams near the crystal surface and optical axis ($x = 0$) after reflection from the upper mirror for various lamp positions δ_{Lamp}. The relative flux in every beam with respect to the power reflected by the lower mirror is specified. Arrows denote the position of the beam waist. Inset: optimum lamp position δ_{Lamp}^{opt} corresponding to light focusing on the crystal surface vs. crystal diameter $D_{crystal}$.

waist of the focused beam. Crystals grown in such a way that their diameter coincides with the position of the waist possess very narrow illumination spots. This effect remains, but only for the beam formed by "ordinary" rays, for $\delta_{Lamp} < \delta_{Lamp}^{crit}$ if the "overlapping" effects occur and two light spots on the crystal surface can be observed. If $D_{1,in}$ and $D_{2,in}$ mirror apertures are considered, the "overlapping" peak is observed only for $\delta_{Lamp} < 8.5\,mm < \delta_{Lamp}^{crit}$ owing to the cut-off effect of the reflected light. The integrated energy flux in every light beam in relation to the flux reflected by the lower mirror is also given in Fig. 10. The dependence of the optimal δ_{Lamp} on crystal diameter $D_{crystal}$ that coincides with the beam waist position is shown in the inset of Fig. 10. Naturally, for $\delta_{Lamp} = 0$ the light is focussed onto the optical axis. To "focus" the light onto the crystal, 10 mm in diameter, δ_{Lamp} should be ~ -5.7 mm. Accordingly, an anomalously high-intensity maximum can be observed for $\delta_{Lamp} = -6$ mm in Fig. 9a.

For $\delta_{Lamp} > 0$, no "exact" light focussing onto the crystal surface can be achieved as shown in Fig. 10. In this case, the calculated waist position of the light beam is negative and the light cone converges continuously toward the optical axis. Nevertheless, the light spot on the crystal surface can be diminished for increasing δ_{Lamp} owing to the decrease of the opening angle of the incident beam accomplished by the cut-off at the $D_{2,out}$ exterior aperture of the upper mirror like for the case of $\delta_{Lamp} = 6$ mm in Fig. 10.

The mirror apertures in the present case are defined by the FZ setup construction and play an important role in forming the irradiation profile and can reduce significantly the total light flux received at the crystal surface. An example of the effect of the mirror apertures on the light profile shaping is shown in Fig. 11a for $\delta_{Lamp} = -3$ mm. Without any apertures, a profile similar to the analytic calculation (Fig. 2) is obtained, i.e. a bell-shaped profile with tails on both sides. The mirror apertures cut-off a part of the radiation distribution, which falls onto the crystal surface. Due to the inner aperture $D_{1,in}$ and the outer aperture $D_{1,out}$ of the lower mirror a narrow ring of 10 mm width on the crystal with 10 mm diameter is illuminated as shown in Fig. 11a. Taking into account the inner aperture $D_{2,in}$ of the upper mirror, leaves an illuminated ring of not more than 5 mm width on the crystal. However, the energy loss caused by the aperture of the upper mirror in this case is less than 25%, which does not restrict opportunities of crystal growth too seriously. Generally, the influence of mirror apertures on the irradiation profile depends on δ_{Lamp} and can become rather complicated.

As already stated above, the lower mirror reflects more than 49% of the total lamp flux in spite of its relative narrow angle range $\sim 60^\circ$ (see Table 1), and this value

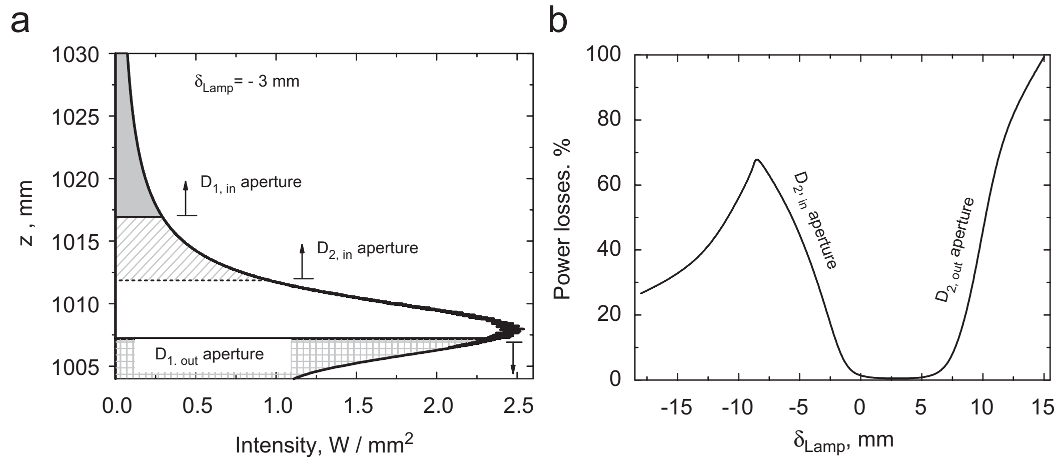

Fig. 11. Effect of apertures of the mirrors on the light profile at the crystal surface for $\delta_{Lamp} = -3$ mm (a). The parts of the light profile cut-off by $D_{1,in}$, $D_{2,in}$ and $D_{1,out}$ apertures are marked by grey colour, oblique hatching and checked hatching, respectively. The dependence of relative power losses at the segment of the upper mirror with respect to the light flux reflected by the lower mirror as a function of lamp position δ_{Lamp} (b). Ranges where $D_{2,in}$ and $D_{2,out}$ apertures raise the light power losses are denoted.

depends only slightly on the lamp position within a range of ± 10 mm. The energy losses caused by apertures of the upper mirror can be very significant and are shown as a function of δ_{Lamp} in Fig. 11b. In the range $-1.5\,\text{mm} < \cap\, \delta_{Lamp} < +7.5$ mm, there are no significant losses and all the light falling onto the upper mirror is reflected to the crystal. For increasing δ_{Lamp}, the outer aperture $D_{2,out}$ plays a significant role and for $\delta_{Lamp} > 15$ mm the whole light flux bypasses the upper mirror and does not reach the crystal surface. For $-9\,\text{mm} < \delta_{Lamp} < -1.5$ mm, there are significant losses due to the inner aperture $D_{2,in}$. But losses are reduced by further decreasing of the lamp position ($\delta_{Lamp} < -9$ mm) because of the "overlapping" ray effect described above. In this case, the incident light rays on the opposite side ($\Theta_3 < 0$) of the upper mirror are reflected toward the crystal.

6. Conclusions

The light propagation in the vertical double-ellipsoid mirror FZ furnace with optical heating was studied within approximations of geometrical optics and an isotropic point source. It was shown that the lamp defocusing δ_{Lamp} along the vertical optical axis is one of prime factors, which determine the character of ray propagation through the setup.

The calculations have proved high optical efficiency of the presented optical configuration, which can exploit about 50% of the light generated by the lamp. It agrees with our practical experience in FZ growth of refractory materials with up to 3000 °C melting temperatures.

It was shown that the light distribution on the reflecting mirrors is far from homogeneous and the major part of radiation can even be concentrated in a very narrow angle range of the mirrors. For lower lamp positions ($\delta_{Lamp} < 0$), the light beam shape is slightly divergent and almost the whole light flux is concentrated near the vertex of the upper mirror. For higher lamp positions ($\delta_{Lamp} > 0$), the beam surface become strongly divergent near the upper mirror and the main part of the light flux reflects from its outer regions.

For $\delta_{Lamp} > 0$, there is a tendency of the light profile on the crystal surface to self-restriction within a narrow range (~5 mm) with extreme sharp boundaries.

One surprising result of our calculation was the split-off of the illumination spots at the crystal surface into two well-separated peaks for the lamp position δ_{Lamp} beyond a critical negative value $\delta_{Lamp} < \delta_{Lamp}^{crit} < 0$. According to our analysis, this phenomenon, which is an inherent property of the two-mirror configuration and does not occur in one-mirror optical furnaces, is caused by the appearance of "ordinary" and "overlapping" rays which arrive at one crystal surface element from different parts of the lower mirror.

For negative values, $\delta_{Lamp} < 0$, a pronounced effect of "focussing" of the converging light into a ring was observed. The "focus" ring diameter depends basically on the lamp position δ_{Lamp}. Crystals with diameters coinciding with the waist of the converging light cone possess very narrow illumination spots with extremely high average intensity.

The calculated flux and ray distributions within the optical configuration will help in practical adjustment and alignment procedures of the lamp in FZ crystal growth processes with predefined heating requirements. In this sense, the present analysis provides a basis for understanding of the vertical double-ellipsoid mirror FZ configuration, which can be extended and supplemented by consideration of other parameters like distance between the mirrors, the effects of diaphragms and by the heat flow analysis of the growth process and the convection in the FZ.

Appendix A

The governing equation of ray transmission from point $\boldsymbol{r}_1$ to $\boldsymbol{r}_2$ according to the straight light ray propagation (not considering diffraction effects) is $\vec{r}_2 = \vec{r}_1 + \vec{k} \cdot t$, where t is a parameter and $\vec{k}$ is a unit wave vector of the propagation direction. The governing equation for the ray reflection from the mirror surface is $\vec{k}_2 = \vec{k}_1 - 2(\vec{k}_1 \cdot \vec{n}_0) \cdot \vec{n}_0$, where $\vec{k}_1$ and $\vec{k}_2$ are the wave vectors before and after the reflection, respectively. The vector $\vec{n}_0$ is a unit normal vector of the mirror surface at the point $\vec{r}_1$.

Placing the origin of the spherical coordinates (θ and φ) at the lamp position, dividing the space into small solid angles $\Delta\Omega_1^{i,j}$ defined by the angles φ_i, φ_{i+1} and θ_j, θ_{j+1}, and applying sequentially the operators of propagation and reflection of a selected ray propagating with the initial wave vector $\vec{k}_1^{i,j}$ it is possible to find its striking points on the lower and the upper mirror and on the crystal surface or at any other plane in the optical system.

The method of direct determination of the intensity distribution over the crystal surface by the solid angle $\Delta\Omega_3^{i,j}$ resulting from the transformation of $\Delta\Omega_1^{i,j}$ after the subsequent reflections of rays from both mirrors seems to be impractical. This method gives an exact result of the irradiation intensity distribution on any predefined surface except of the regions where the geometrical optics does not work. For example, near the points where the "exact" focussing area within approximation of geometry optics, intersects the crystal surface an unrealistic extremely high intensity results. According to our estimations, these regions, where the simple ray optics does not work but diffraction theory should be taken into account, are in the order of 5–50 μm for the present optical system.

Therefore, the so-called method of a radiation detector array was applied for calculation of intensity profiles over specified surfaces in the present optical system. The investigated surface is subdivided into a network with cells acting as optical sensors for the light intensity. The area of the cell (n, m)defined by the net partition is $S_{\text{Cell}}^{m,n}$. The signal of this cell is proportional to the average incident light flux (but not to the average light intensity), and is determined as

$$I^{n,m} = \frac{\sum_{k=1}^{N_{\text{P}}} \Delta P^k}{S_{\text{Cell}}^{n,m}},$$

where ΔP^k ($k = 1, 2, \ldots, N_{\text{P}}$) is the irradiation flux within the solid angle $\Delta\Omega_3^k$ that intersects the cell $S_{\text{Cell}}^{n,m}$ and N_{P} is the number of the solid angle elements. This integration process permits a calculation of the radiation distribution close to the real setup geometry and it diminishes the effects of the non-linear optics near the areas with exact light focusing under the conditions $S_{\text{Cell}}^{n,m} > 50\,\mu\text{m}$ and $N_{\text{P}} \gg 1$. This method is widely used in commercial program packages such as ZEMAX for mathematical analysis of various optical systems. For example, the radiation detector array at the crystal coincides with its surface and has a cell size around 250–500 μm, depending on the requirements.

Appendix B

The solid angle elements with respect to the origins positioned in F1 to F4 points between the angles θ and $\theta + \mathrm{d}\theta$ and φ and $\varphi + \mathrm{d}\varphi$ are $\mathrm{d}\Omega_{1,3} = \sin\theta_{1,3}\,\mathrm{d}\theta_{1,3}\,\mathrm{d}\varphi$, respectively. Angles θ_1 and θ_3 are shown in Fig. 1b. If transmission and reflection losses are negligible, the total flux emitted by a point source within $\mathrm{d}\Omega_1$ is received in $\mathrm{d}\Omega_3$ and the flux density in $\mathrm{d}\Omega_3$ is

$$q_3 = \frac{\mathrm{d}\Omega_1}{\mathrm{d}\Omega_3}\frac{P_0}{4\pi},$$

where P_0 is total lamp power. The light intensity produced by the solid angle $\mathrm{d}\Omega_3$ reflected from the upper mirror on the cylindrical surface with diameter D_{crystal} is:

$$I(\theta, \varphi) = q_3 \frac{\mathrm{d}\Omega_3}{\mathrm{d}S_{\text{crystal}}},$$

where $\mathrm{d}S_{\text{crystal}}$ is the crystal surface element contained in the solid angle $\mathrm{d}\Omega_3$. After a simple mathematical transformation, we obtain the intensity value at the ring of the crystal surface defined by θ_3:

$$I = \frac{P_0}{\pi D_{\text{crystal}}}\left(\frac{\mathrm{d}\theta_1}{\mathrm{d}\theta_3}\right)^2 \sin^3\theta_3. \tag{B.1}$$

From the geometry and ellipse features, the following equations can be obtained in the same way as in Ref. [24]:

$$\frac{\mathrm{d}\theta_1}{\mathrm{d}\theta_3} = \frac{1 - e_2^2}{1 - e_1^2}\frac{1 + e_1^2 + 2e_1\cos\theta_1}{1 + e_2^2 + 2e_2\cos\theta_3}, \tag{B.2}$$

$$\cos\theta_1 = \frac{(1 + e_1^2)\cos\theta_2 - 2e_1}{(1 + e_1^2) - 2e_1\cos\theta_2}, \tag{B.3}$$

$$\cos\theta_2 = \frac{(1 + e_2^2)\cos\theta_3 + 2e_2}{(1 + e_2^2) + 2e_2\cos\theta_3}, \tag{B.4}$$

$$\cos\theta_3 = \frac{z - 2p_2}{\sqrt{(z - 2p_2)^2 + \left(\frac{D_{\text{crystal}}}{2}\right)^2}}, \tag{B.5}$$

where e_1 and e_2 are the eccentricities of the lower and upper ellipsoids, respectively, and $2p_2$ corresponds to the absolute position of the focal point F4. All these values are given in Table 1.

By subsequent substitution of Eqs. (B.2)–(B.5) into Eq. (B.1), we obtain the analytical form of the light intensity on the crystal surface positioned at the focal point F4 of the upper mirror.

References

[1] T. Akashi, K. Matumi, T. Okada, T. Mizutani, IEEE Trans. Magn. 3 (1969) 285.

[2] A. Eyer, B.O. Kolbesen, R. Nitsche, J. Crystal Growth 27 (1982) 145.

[3] C.H. Lee, N. Kaneko, S. Hosoya, K. Kurahashi, S. Wakimoto, K. Yamada, Y. Endoh, Supercond. Sci. Technol. 11 (1998) 891.
[4] C.W. Lan, C.H. Tsai, J. Crystal Growth 173 (1997) 561.
[5] Four mirror type optical floating zone furnace, Crystal system Inc., Technical Report FZ-E-002, 1992.
[6] T. Mizutani, K. Matsumi, H. Makino, Y. Yamamoto, T. Kato, Single crystal growing apparatus using infrared heating, NEC Res. Dev. 33 (1974) 86.
[7] K. Hatta, M. Higuchi, J. Takahashi, K. Kodaira, J. Crystal Growth 163 (1996) 279.
[8] A. Revcolevschi, U. Ammerahl, G. Dhalenne, J. Crystal Growth 198–199 (1999) 593.
[9] G. Balakrishnan, M.R. Lees, D. MK. Paul, J. Crystal Growth 256 (2003) 206.
[10] J.G. Bednorz, H. Arend, J. Crystal Growth 67 (1984) 660.
[11] P. Dold, M. Schweizer, A. Cröll, K.W. Benz, J. Crystal Growth 237–239 (2002) 1671.
[12] P.I. Nabokin, D. Souptel, A.M. Balbashov, J. Crystal Growth 250 (2003) 397.
[13] D. Souptel, G. Behr, A.M. Balbashov, J. Crystal Growth 236 (2002) 583.
[14] Ch. Kloc, S.-W. Cheong, P. Matl, J. Crystal Growth 191 (1998) 294.
[15] D. Souptel, G. Behr, A. Kreyssig, W. Löser, J. Crystal Growth 276 (2005) 652.
[16] D. Souptel, G. Behr, W. Löser, K. Nenkov, G. Fuchs, J. Crystal Growth 275 (2005) e91.
[17] D. Souptel, A. Leithe-Jasper, W. Löser, W. Schnelle, H. Borrmann, G. Behr, J. Crystal Growth 273 (2004) 311.
[18] D. Souptel, G. Behr, W. Löser, A. Teresiak, S. Drotziger, C. Pfleiderer, J. Crystal Growth 269 (2004) 606.
[19] D. Souptel, G. Behr, L. Ivanenko, H. Vinzelberg, J. Schumann, J. Crystal Growth 244 (2002) 296.
[20] D. Shulyatev, S. Karabashev, A. Arsenov, Ya. Mukovskii, S. Zverkov, J. Crystal Growth 237–239 (2002) 810.
[21] D. Shulyatev, S. Karabashev, A. Arsenov, Ya. Mukovskii, J. Crystal Growth 198–199 (1999) 511.
[22] G. Behr, W. Löser, M.-O. Apostu, W. Gruner, M. Hücker, L. Schramm, D. Souptel, A. Teresiak, J. Werner, Cryst. Res. Technol. 40 (2005) 21.
[23] D. Rivas, C. Vázquez-Espí, J. Crystal Growth 223 (2001) 433.
[24] P.J. Hart, Am. J. Opt. Soc. Am. 48 (1958) 637.
[25] D. Rivas, C. Vázquez-Espí, Adv. Space Res. 29 (2002) 575.
[26] A.M. Balbashov, A.Yu. Lebedev, S.G. Pavlova, V.E. Bakhteuzov, Acta Phys. Pol. A 68 (1985) 457 (in Russian).